Appl. Phys. A (2004)
DOI: 10.1007/s00339-004-2713-z

Applied Physics A
Materials Science & Processing

Y.K. SU[1,2]
C.M. SHEN[2]
T.Z. YANG[2]
H.T. YANG[2]
H.J. GAO[2]
H.L. LI[1,✉]

The dependence of Co nanoparticle sizes on the ratio of surfactants and the influence of different crystal sizes on magnetic properties

[1] Department of Chemistry, Lanzhou University, Lanzhou 730000, P.R. China
[2] Nanoscale Physics and Devices Laboratory, Institute of Physics, Chinese Academy of Sciences, Beijing 100080, P.R. China

Received: 10 November 2003/Accepted: 6 February 2004
Published online: 4 May 2004 •

ABSTRACT Monodisperse cobalt nanoparticles were synthesized by high-temperature reduction of solution-phase cobalt chloride in the presence of a pair of surfactants, oleic acid and triphenylphosphine. Highly ordered two-dimensional superlattices of passivated cobalt nanoparticles were formed by a self-assembly technique. Analysis by X-ray diffraction, UV-vis absorption spectroscopy and transmission electron microscopy demonstrated that the size of the cobalt nanocrystals could be tuned by tailoring the concentration ratio of the two surfactants. In addition, the influence of different crystal sizes on magnetic properties of Co nanocrystals was also investigated.

PACS 75.60.Nt; 75.50.Tt

1 Introduction

Magnetic nanocrystals (NCs) exhibit finite size effects that may provide insight into ultra-high-density magnetic information storage [1–5]. In order to probe the fundamental size-dependent properties of magnetic NCs, it is important to prepare size-tunable monodisperse magnetic nanoparticles with controllable internal structures [6, 7]. A number of methods can be used to control NC size, with notable examples including adjusting the reaction temperature and tailoring the ratio of the concentration of reagents to that of surfactants [8–10]. The chemistry of the surface agent provides another effective strategy for controlling NC size. However, less work has been presented on this subject in the past [11, 12].

In this paper, we describe the synthesis of cobalt nanoparticles (NPs) by reduction of cobalt chloride with lithium triethyl boron hydride ($LiBEt_3H$) in the presence of triphenylphosphine (TPP) and oleic acid (OA) [13, 14]. The TPP and OA are employed as stabilizers to control particle growth, stabilize the particles and prevent the particles from oxidation. Different from the previous literature, TPP, which has a triangular pyramid structure, has been used instead of tributylphosphine or trioctylphosphine. The steric hindrance of the phenyl group in TPP in the transverse direction is larger than that of the alkyl chain, so that it can be used to control cobalt NPs with small size. Through judicious adjustment of the ratio of the TPP to OA stabilizers, the size of NCs can be controlled. After the size range of the cobalt NPs is further narrowed through size-selective precipitation [15], two-dimensional (2D) superlattice structures are obtained by controlled solvent evaporation. The size-tunable NCs are investigated with X-ray diffraction (XRD), UV-vis absorption spectroscopy and transmission electron microscopy (TEM). Magnetic properties of Co NCs of different crystal sizes are investigated with superconducting quantum interference device (SQUID) magnetometry.

✉ Fax: +86-931/891-2582, E-mail: lihl@lzu.edu.cn

2 Experiments

2.1 *Nanocrystal synthesis*

Cobalt chloride (anhydrous), OA, TPP, diphenylether and $LiBEt_3H$ were purchased from Acros. Cobalt NPs were fabricated using a method similar to that of Sun and Murray [13]. They proposed that a temporal separation of the nucleation and the growth stages was required for the production of a monodisperse colloid. 0.13 g cobalt chloride (anhydrous), 0.32 ml OA and 30 ml diphenylether were mixed under nitrogen atmosphere and heated to nearly 100 °C. Then 0.79 g TPP was added and heated to ∼ 210 °C. The Co NPs began to emerge with the injection of 2 ml diphenylether superhydride ($LiBEt_3H$) into the vigorously stirred solution. The color gradually changed from blue to black during the first minute as the Co NCs nucleated and began to grow. The reaction was held at ∼ 210 °C for 30 min. Then the dispersion of Co NCs was cooled to room temperature. After that, 20 ml of ethanol was poured into the black solution to disperse the cobalt NPs. The supernatant was discarded by centrifugation, and the precipitate was again dispersed in 15 ml heptane with a drop of OA to ensure the stability of the NPs.

2.2 *Characterization of samples*

The structure of Co NCs was investigated by a Rigaku D/MAX-200 X-ray diffractometer with Cu K_α radiation ($\lambda = 1.5406$ Å). UV-vis absorption spectra of the NC dispersions in heptane were measured using a Shimadzu UV-1601 PC double-beam spectrophotometer. Slow evaporation of the heptane dispersion of cobalt NPs spread on a carbon-film-coated copper grid allows well-organized superlattice

structures to be formed. TEM images of the superlattices were obtained using a JEM 200CX operating at 200 kV. Magnetic measurement was conducted in a MPMS-5 superconducting quantum interference device (SQUID) magnetometer.

3 Results and discussion

3.1 *Structural analysis*

The element cobalt has long been known to have two stable crystal line structures: close-packed hexagonal (hcp) and face-centered cubic (fcc). Both phases can exist at room temperature. The fcc structure is thermodynamically preferred above 450 °C and the hcp phase is favored at lower temperatures. For small particles, however, the fcc structure appears to be preferred even below room temperature [16].

In our experiment, the crystalline structure of Co NCs is neither fcc nor hcp; it is a new phase with the symmetry found in the ß phase of the elemental Mn. This crystalline structure has been designated as the ε phase of cobalt (ε-Co) [17]. Figure 1 shows the diffraction patterns of Co NCs. The three reflection peaks are observed at $2\theta = 44.5, 47.1$ and 49.5, corresponding to (221), (310) and (311) planes of the ε-Co lattice plane, respectively. It is in good agreement with the ε-Co structure observed by Sun and Murray [13]. No distinct peak corresponding to CoO or CoB phases is detected, indicating that a single ε-Co phase is obtained.

In the XRD pattern, the diffraction peaks gradually become sharp and the intensity of the peaks increases as the TPP/OA ratio increases, revealing an increase of the size of Co NCs. Therefore, by tuning the molar ratio of TPP to OA, we can control the size of Co NCs.

3.2 *The size control of* Co *NCs*

In general, adjusting the temperature and the metal-precursor-to-surfactant ratio can control NP size. Higher temperatures and larger metal-precursor-to-surfactant ratios produce larger NPs [18]. The chemistry of the surface agent can also be chosen to control NC size. During NC growth, the surfactants adsorb reversibly to NP surfaces and provide a dynamic organic shell that mediates particle growth, stabilizes the particles and limits oxidation after synthesis [15]. In this experiment, we have used a pair of surfactants – triphenylphosphine (TPP) and oleic acid (OA) – to control particle growth. The OA binds tightly to the particle surface during synthesis that hinders the particle from growing; the TPP reversibly coordinates neutral metal surface sites that favor rapid growth. Judicious adjustment of the ratio of TPP (weakly bound) to OA (tightly bound) stabilizers can control the size of NCs. Figure 2 shows UV-vis absorption spectra of Co NCs prepared at different TPP/OA molar ratios. It is observed that the absorption peak of the spectrum (a) is at about 260 nm and the absorption position gradually shifts to higher wavelength (red shift) with increasing TPP/OA molar ratios, indicating that the sizes of the Co NCs increase with increasing TPP/OA molar ratios. By this method, we can tune the average size of the particles.

3.3 *The self-assembly of* Co *NCs*

The TEM images further illustrate that different sizes of Co nanocrystals can be obtained at different TPP/OA molar ratios. When the TPP/OA molar ratios equal 3 : 1, 5 : 1 and 7 : 1, the sizes of the Co NCs are 6.5 nm (Fig. 3a), 8 nm (Fig. 3b) and 9.5 nm (Fig. 3c), respectively. In Fig. 3, the ε-Co NCs are uniform in both size and shape, which makes them self-assemble into a two-dimensional monodisperse film [19, 20]. The hexagonal arrangement of the nanocrystal superlattice formation is driven by surface tension, attractive van der Waals forces and magnetic interaction between superparamagnetic particles. This assembly process is reversible by immersing the sample in heptane. The upper inset in Fig. 3a shows the 2D Fourier-transform power spectrum of the zoomed area, which shows the hexagonal close-packed (hcp) structure of the ordered nanoparticles.

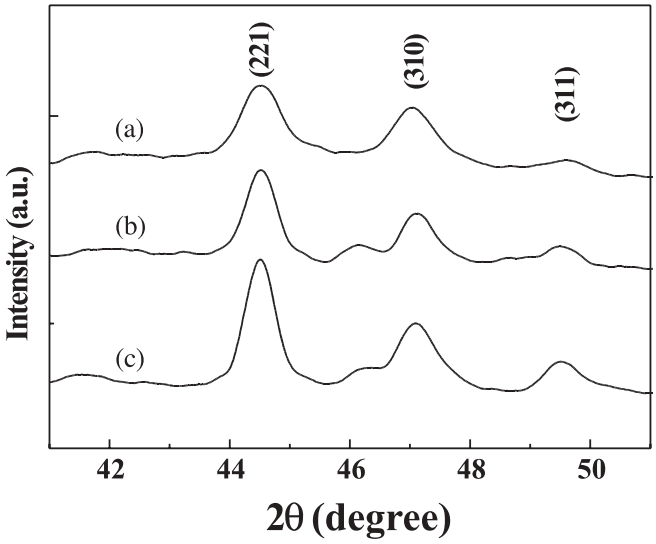

FIGURE 1 XRD pattern of Co NCs at different concentration ratios of TPP to OA, a = 3 : 1, b = 5 : 1, c = 7 : 1. The reflection peaks of Co NCs gradually become sharp, indicating that the size of the Co NCs gradually increases

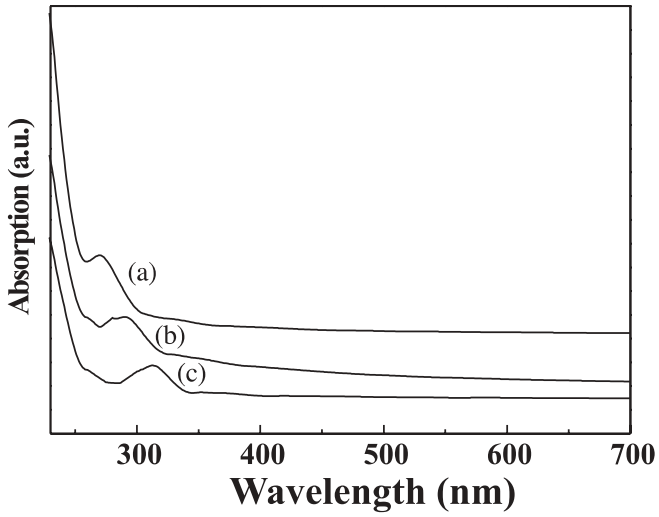

FIGURE 2 UV-vis spectra of the Co NCs at different ratios of TPP to OA, a = 3 : 1, b = 5 : 1, c = 7 : 1. The absorption position gradually shifts to higher wavelength, indicating that the size of the Co NCs gradually increases

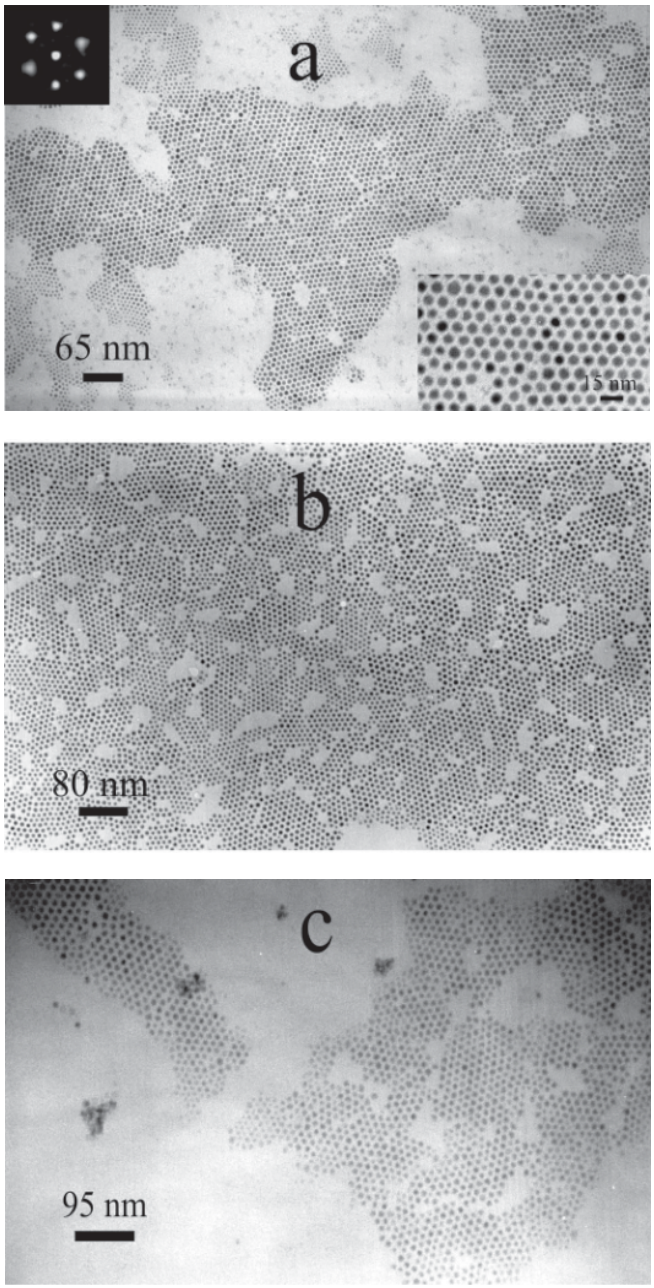

FIGURE 3 TEM image of two-dimensional superlattice of Co NCs at different concentration ratios of TPP to OA: **a** 6.5 nm at TPP/OA= 3 : 1, **b** 8 nm at TPP/OA = 5 : 1, **c** 9.5 nm at TPP/OA = 7 : 1; the *upper inset* of (**a**) shows the 2D Fourier-transform power spectrum of the TEM image and the *lower inset* shows highly ordered Co nanoparticles in the selected area

3.4 *The magnetic properties of* Co *NCs*

The magnetic properties of different sizes of Co NCs were measured with a SQUID magnetometer using a standard airless procedure. All the synthesized magnetic NPs were below the critical size at which a particle becomes a single magnetic domain and displays superparamagnetism [21]. The temperature dependence of the magnetization was measured in a 10-Oe magnetic field from 5 K to 300 K to determine the blocking temperature, T_B, a maximum in the magnetization, using the zero-field-cooling (ZFC) procedure. The relationship between the blocking temperature and the particle size is shown in Fig. 4. According to the measurement results, the blocking temperature T_B of 6.5-, 8- and 9.5-nm Co NPs is 60, 100 and 150 K, respectively. The blocking temperature increases as the particle size increases, which implies a series of good samples [22]. The blocking temperature should roughly satisfy the following relationship:

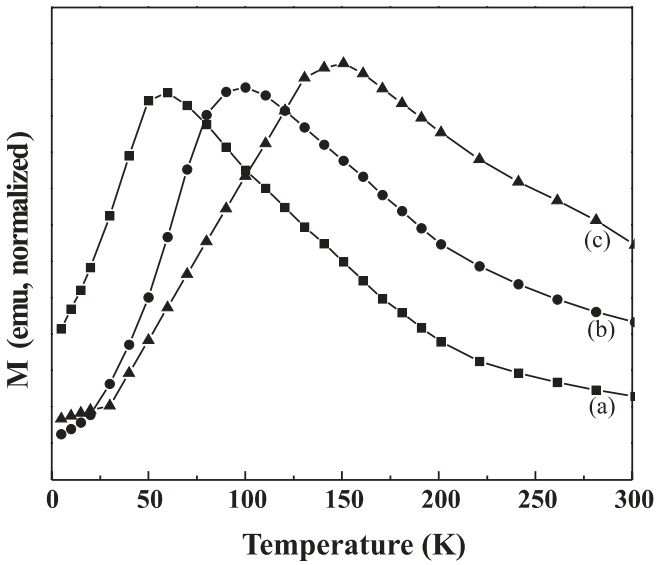

FIGURE 4 Zero-field-cooled (ZFC) magnetization for (a) 6.5-nm, (b) 8-nm and (c) 9.5-nm Co NCs

$$T_B = KV/30k_B\,, \tag{1}$$

where K is the anisotropy constant, k_B Boltzmann's constant and V the average volume of the particle. The anisotropy constant of the Co particles of 6.5, 8 and 9.5 nm is 2.1×10^6, 1.5×10^6 and 1.3×10^6 erg/cm^3, respectively. As the particle size decreased, the anisotropy constant increased. The observed enhancement cannot be attributed to shape anisotropy, since TEM shows our particles to be fairly spherical. Therefore, the most reasonable explanation is surface anisotropy. It is well known that there is a large fraction of Co atoms on the surface of NPs, which results in a large anisotropy [23].

Figure 5a, b and c show the size-dependent magnetization vs. applied magnetic field (M vs. H) hysteresis loops at 5 K for ε-Co NCs of 6.5 nm, 8 nm and 9.5 nm in diameter, respectively. Below the blocking temperature, the magnetic moment of the NC is pinned along an 'easy axis' and is ferromagnetic. Hence, the reversal of the magnetic moment along the easy axis implies the jumping over an energetic barrier, which is proportional to the product of the anisotropy constant (K) and the volume of the NC (V) [24]. As the size of the NC decreases, the width of the hysteresis loop decreases with the decrease of the energetic barrier KV. The coercivity H_c of 6.5-, 8- and 9.5-nm Co NCs is 247, 386 and 838 Oe, respectively. H_c increases with increasing size of cobalt NCs, which is the behavior of single-domain particles caused by thermal effects. The sharp drop in saturation magnetization (relative to that for bulk Co) with the decrease of the NC's size results from the increase in the NP surface-to-volume ratio [25]. Figure 5c and d show the hysteresis loops of 9.5-nm ε-Co at 5 K and 290 K, respectively. At 290 K, above the block-

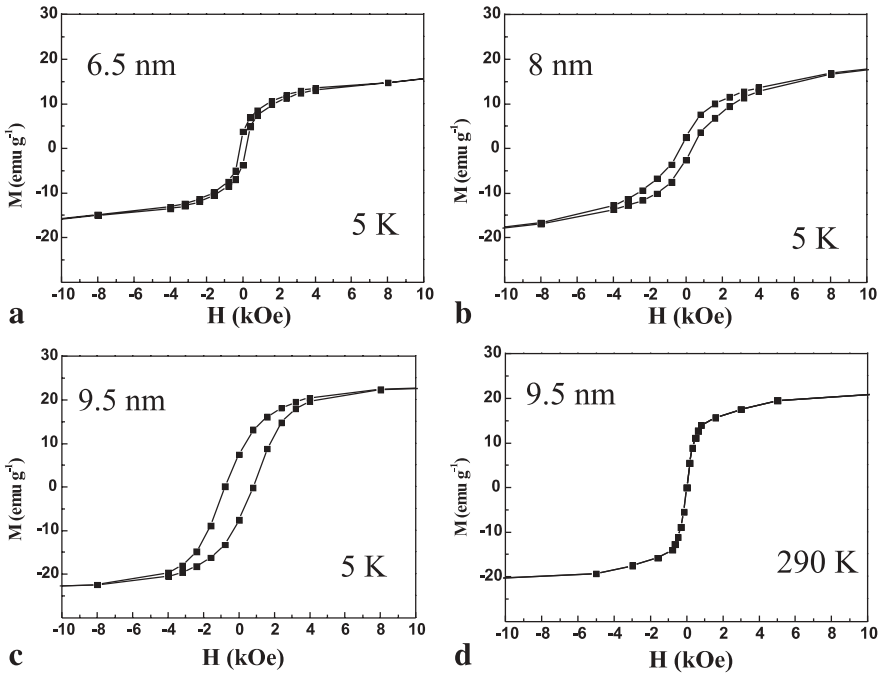

FIGURE 5 Magnetization vs. field (M vs. H) hysteresis loops at 5 K for Co NCs with **a** 6.5 nm, **b** 8 nm and **c** 9.5 nm. Comparison of M vs. H loops for 9.5-nm Co NCs at **c** 5 K and **d** 290 K

ing temperature, the magnetic anisotropy energy barrier of the single-domain particles is overcome by thermal energy and superparamagnetism occurs.

4 Conclusions

Monodisperse cobalt NCs with β-Mn phase have been prepared employing high-temperature-solution phase reduction. The long-range-ordered and close-packed nanoparticle arrays are obtained by self-assembly. The controlled sizes of the cobalt NCs are presented by adjusting the concentration ratio of TPP to OA stabilizers. Magnetic properties of different-size Co NCs supported the size dependence fairly well. These results will be helpful for controlling the size of Co NPs and understanding NC finite size effects for further applications to spin-transport devices.

ACKNOWLEDGEMENTS This work was supported by the Natural Science Foundation of China (Grant No. 60276041).

REFERENCES

1 E. Bar-Sadeh, Y. Goldstein, C. Zhang, H. Deng, B. Abeles, O. Millo: Phys. Rev. B **50**, 8961 (1994)
2 H.J. Gao, K. Sohlberg, Z.Q. Xue, H.Y. Chen, S.M. Hou, L.P. Ma, X.W. Fang, S.J. Pennycook: Phys. Rev. Lett. **84**, 1780 (2000)
3 A.N. Korotkov, R.H. Chen, K. Likharev: J. Appl. Phys. **78**, 2520 (1995)
4 R.P. Andres, T. Bein, M. Dorogi, S. Feng, J.I. Henderson, C.P. Kubiak, W. Mahoney, R.G. Osifchin, R. Reifenberger: Science **272**, 1323 (1996)
5 Y. Shi, K. Saito, H. Ishikura, T. Hiramoto: J. Appl. Phys. **84**, 2358 (1998)
6 H.T. Yang, C.M. Shen, Y.K. Su, T.Z. Yang, H.J. Gao: Appl. Phys. Lett. **82**, 4729 (2003)
7 M.J. Feldstein, C.D. Keating, Y.H. Liau, M.J. Natan, N.F. Sherer: J. Am. Chem. Soc. **119**, 6638 (1997)
8 S.T. He, S.S. Xie, J.N. Yao, S.J. Pang: Appl. Phys. Lett. **81**, 50 (2002)
9 Z.L. Wang: Aust. J. Chem. **54**, 153 (2001)
10 C.M. Shen, Y.K. Su, H.T. Yang, T.Z. Yang, H.J. Gao: Chem. Phys. Lett. **373**, 39 (2003)
11 A.P. Alivisatos: Science **271**, 933 (1996)
12 L. Clarke, M.N. Wybourne, L.O. Brown, J.E. Hutchison, M. Yan, S.X. Cai, J.F.W. Keana: Semicond. Sci. Technol. **13**, A111 (1998)
13 S.H. Sun, C.B. Murray: J. Appl. Phys. **85**, 4325 (1999)
14 V.F. Putes, K.M. Krishan, A.P. Alivisatos: Science **291**, 2115 (2001)
15 C.B. Murray, S.H. Sun, W. Gaschier, H. Doyle, T.A. Betley, C.R. Kagan: IBM J. Res. Dev. **45**, 47 (2001)
16 Power diffraction file PDF-2 database sets 1–44 (1994)
17 D.P. Dinega, M.G. Bawendi: Angew. Chem. Int. Ed. **38**, 1788 (1999)
18 C.B. Murray, S.H. Sun, H. Doyle, T. Betley: MRS Bull. **26**, 985 (2001)
19 S.T. He, J.N. Yao, P. Jiang, D.X. Shi, H.X. Zhang, S.S. Xie, S.J. Pang, H.J. Gao: Langmuir **17**, 1571 (2001)
20 S. Sun, C.B. Murray, D. Weller, L. Folks, A. Moser: Science **287**, 1989 (2000)
21 D.L. Leslie-Pelecky, R.D. Rieke: Chem. Mater. **8**, 1770 (1996)
22 J.P. Chen, C.M. Sorensen, K.J. Klabunde, G.C. Hadjipanayis: Phys. Rev. B **51**, 11 527 (1995)
23 F. Bodker, S. Morup, S. Linderoth: Phys. Rev. Lett. **72**, 282 (1994)
24 J.-F. Hochepied: Online Nanotechnol. J. **I**, Issue 1, October (2000)
25 G.A. Held, G. Grinstein, H. Doyle, S. Sun, C.B. Murray: Phys. Rev. B **64**, 012 408 (2001)